Title

Flux rewiring enables native D-glucosamine production in Escherichia coli

Journal

METABOLIC ENGINEERING, 98

ISSN

1096-7176

Authors

Palur, Dileep Sai Kumar

Bait, Amey

Luu, Bryant

et al.

Publication Date

2026-11-01

DOI

10.1016/j.ymben.2026.102526

Flux Rewiring Enables Native D-Glucosamine Production in *Escherichia coli*

Dileep Sai Kumar Palur[1], Amey Bait[1], Bryant Luu[2], Ian C. Anderson[3], John Didzbalis[4], Justin B. Siegel[1,2,5,6], and Shota Atsumi[1,2*]

[1]Department of Chemistry, University of California, Davis, Davis, CA, 95616, USA

[2]Biochemistry, Molecular, Cellular, and Developmental Graduate Group, University of California, Davis, Davis, CA, 95616, USA

[3]Integrative Genetics and Genomics, University of California, Davis, Davis, CA, 95616, USA

[4]Mars, Incorporated, 6885 Elm Street, McLean, VA 22101, USA

[5]Genome Center, University of California, Davis, Davis, CA 95616, USA.

[6]Department of Biochemistry and Molecular Medicine, University of California, Davis, Sacramento, CA 95616, USA.

*To whom correspondence may be addressed: E-mail: satsumi@ucdavis.edu

Abstract

D-Glucosamine is an industrially important amino sugar used in pharmaceuticals, nutraceuticals, and functional materials, yet its production remains dominated by chemical extraction from chitinous biomass, raising sustainability and allergen concerns. *Escherichia coli* natively synthesizes D-glucosamine directly from D-glucose through endogenous metabolism, revealing an underutilized amino sugar biosynthetic capability. Building on this native pathway, D-glucosamine production was enhanced through targeted genetic modifications and systematic optimization of nitrogen metabolism and cultivation conditions, reaching 9.2 g L^{-1} under shake-flask conditions. This work extends a phosphorylation–dephosphorylation strategy previously developed for neutral rare sugars to amino sugar biosynthesis, demonstrating the broader applicability of this metabolic design principle. Phosphatase identity emerged as a key control point for product formation: YbiV was the most effective phosphatase for selective D-glucosamine production, whereas alternative phosphatases redirected flux toward D-sedoheptulose. This enzyme-dependent flux partitioning further enabled tunable co-production of D-glucosamine and D-sedoheptulose. Native amino sugar biosynthesis in *E. coli* provides a controllable framework for producing chemically distinct sugars through endogenous metabolism and establishes a generalizable strategy for engineering amino sugar and other nitrogen-containing metabolite biosynthesis.

Keywords: Rare sugars, D-Glucosamine, Metabolic Engineering

Highlights

- *Escherichia coli* natively synthesizes D-glucosamine from D-glucose
- Endogenous amino sugar biosynthesis is uncovered and enhanced in *E. coli*
- Phosphorylation–dephosphorylation enables amino sugar production
- YbiV phosphatase enables selective D-glucosamine formation
- Phosphatase identity enables tunable co-production with D-sedoheptulose

1. Introduction

D-Glucosamine is a high-value amino sugar with broad applications in pharmaceuticals, nutraceuticals, and functional materials (Protity and Zhou, 2025). It serves as a key precursor for diverse bioactive compounds (Zhang et al., 2025) and polymeric materials (Bordegé et al., 2011). It is also widely incorporated into dietary supplements for both human and animal health, particularly in pet food and veterinary formulations intended to support joint health and alleviate symptoms associated with osteoarthritis (Bhathal et al., 2017). Beyond health-related applications, D-glucosamine has attracted growing interest as a food-relevant ingredient because it participates in Maillard reactions that generate flavor-active compounds and influence sensory attributes such as sweetness and umami (Hong and Betti, 2016; Yu et al., 2022). Reflecting its expanding range of applications, the global glucosamine market was estimated at USD 1.10 billion in 2024 and is projected to grow at a compound annual growth rate of 5.63% from 2025 to 2034 (“Glucosamine Market Size,” 2025). Despite its widespread use, industrial production of D-glucosamine remains dominated by chemical extraction from chitinous biomass derived from crustacean shells (Bertuzzi et al., 2018; Zhang et al., 2025). This process has motivated interest in alternative production routes that are scalable, sustainable, and independent of animal-derived feedstocks, while also addressing concerns related to allergenicity and environmental impact (Ahuja et al., 2025; Protity and Zhou, 2025).

Beyond extractive chemical routes, enzymatic approaches have also been explored for D-glucosamine synthesis, typically relying on the amination of sugar intermediates using nitrogen donors (Guan et al., 2024; Meng et al., 2020) or enzymatic

hydrolysis of chitosan (Gao et al., 2023; Pan et al., 2011). While enzymatic methods offer improved selectivity and milder reaction conditions relative to chemical extraction, they often require high concentrations of ammonia to drive conversion, which introduces challenges related to toxicity, corrosion, downstream separation, and environmental impact (Guan et al., 2024; Meng et al., 2020). These limitations have hindered the large-scale implementation of enzymatic D-glucosamine production and have motivated interest in microbial production systems that generate D-glucosamine directly from renewable carbon sources through cellular metabolism.

Microbial fermentation has emerged as a sustainable approach for chemical production from renewable feedstocks (Cowan et al., 2023), motivating efforts to produce D-glucosamine using engineered microorganisms. In *Escherichia coli*, early strategies relied on overexpression of *glmS* encoding for L-glutamine–D-fructose-6-phosphate aminotransferase to increase glucosamine-6-phosphate (GlcN6P) formation from D-fructose-6-phosphate (F6P) (Deng et al., 2005; Teplyakov et al., 2002). Later studies demonstrated that glucosamine accumulation is highly sensitive to cultivation conditions, particularly oxygen availability, indicating a strong dependence on respiratory and redox metabolism that complicates process robustness (Chen et al., 2012). More extensive pathway engineering later combined deletion of D-glucosamine and N-acetylglucosamine catabolic genes (*nanE* and *murQ*) (Plumbridge and Vimr, 1999; Uehara et al., 2006), reduction of GlmU acetyltransferase activity (Mengin-Lecreulx and van Heijenoort, 1994), and co-expression of *glmS* with *gna1* (Deng et al., 2006b) to enhance extracellular D-glucosamine accumulation (Li et al., 2020). However, these interventions perturbed UDP-GlcNAc homeostasis, leading to impaired cell-

envelope biosynthesis, reduced growth, and diminished glucose uptake (Li et al., 2020). Beyond bacterial systems, implementation of analogous biosynthetic pathways in *Saccharomyces cerevisiae* further highlighted host-dependent constraints on glucosamine production (Yang et al., 2025). Collectively, prior studies reveal persistent challenges, including the absence of an identified phosphatase capable of efficiently converting GlcN6P to free D-glucosamine, the tight coupling of amino sugar biosynthesis with essential cell-envelope metabolism, and the chemical instability of D-glucosamine in cultivation media. Consequently, many microbial production efforts have shifted toward the more stable derivative N-acetyl-D-glucosamine rather than D-glucosamine itself (Yang et al., 2025).

In parallel, filamentous fungi have been explored as alternative hosts for D-glucosamine production, where accumulation occurs predominantly as a biomass-associated product rather than through targeted metabolic engineering (Hsieh et al., 2007; Zhang et al., 2012). In these systems, D-glucosamine formation is closely linked to fungal growth, cell-wall biosynthesis, and chitin or chitosan turnover, and production is typically enhanced through process-level interventions such as dissolved oxygen control and modulation of pellet morphology rather than through deliberate redistribution of metabolic flux (Zhang et al., 2012). Comparative analyses across *Aspergillus*, *Monascus*, and *Rhizopus* species further demonstrated that D-glucosamine productivity correlates strongly with growth kinetics and biomass composition, with limited evidence for selective enhancement of amino sugar biosynthesis independent of biomass accumulation (Hsieh et al., 2007). While these fungal platforms can achieve high apparent D-glucosamine accumulation, production remains intrinsically coupled to

biomass formation, limiting opportunities for independent control of carbon partitioning, product selectivity, and metabolic engineering.

In this study, we sought to establish a biosynthetic route for D-glucosamine production in *E. coli* by leveraging endogenous metabolic capacity rather than constructing heterologous pathways or perturbing essential cell-envelope metabolism. We focused on identifying and amplifying native reactions linking central carbon metabolism to amino sugar biosynthesis, with particular emphasis on controlling flux through GlcN6P formation and dephosphorylation. A key objective was to evaluate endogenous sugar phosphatases as functional control points for directing product formation despite their inherent promiscuity. We further investigated the role of nitrogen assimilation in constraining amino sugar biosynthesis and developed strain engineering strategies to alleviate these limitations. Together, these efforts establish a genetically defined D-glucosamine production platform and provide new insights into the endogenous metabolic network supporting amino sugar biosynthesis in *E. coli*. More broadly, this work demonstrates how latent biosynthetic capabilities can be identified and engineered to produce amino sugars and other nitrogen-containing metabolites.

2. Methods

2.1. Reagents

All enzymes involved in the molecular cloning experiments were purchased from New England Biolabs (NEB). All synthetic oligonucleotides were synthesized by Integrated DNA Technologies. Sanger Sequencing and whole plasmid sequencing was

provided by Genewiz. D-Glucosamine and D-sedoheptulose were purchased from Tokyo Chemical Industry. D-Glucose was purchased from Fisher Scientific.

2.2. Strains and Plasmids

All strains and plasmids used in this study are listed in **Table 1** and **2**, respectively. All oligonucleotides are listed in **Table S1**. Plasmids were constructed using sequence and ligation independent cloning (SLIC) (Li and Elledge, 2007). The constructed plasmids were verified via sequencing. A guide to the construction of plasmids used in this study is detailed in **Table S2**.

Genome modifications such as gene deletion and gene insertion were constructed using CRISPR-Cas9-mediated homologous recombination (Jiang et al., 2015). Linear DNA repair fragments for gene deletions and insertions were constructed by amplifying genomic or plasmid DNA via PCR assembly (Xiong et al., 2004). Plasmids encoding sgRNA for CRISPR-Cas9-mediated homologous recombination were constructed using Q5 site-directed mutagenesis (New England Biolabs) using pTargetF plasmid (Addgene #62226) as a template. All genomic modifications were verified via sequencing. A guide to the CRISPR-Cas9-mediated gene modifications used in this study is detailed in **Table S3**.

2.3. Culturing conditions

Overnight cultures were grown at 37 °C in 3 mL of Luria-Bertani (LB) medium with appropriate antibiotics. Antibiotic concentrations were as follows: spectinomycin (50 μg mL^{-1}), ampicillin (200 μg mL^{-1}), kanamycin (50 μg mL^{-1}), gentamycin (15 μg mL^{-1}). M9 minimal media consists of 33.7 mM Na_2HPO_4, 22 mM KH_2PO_4, 8.6 mM NaCl, 9.4 mM NH_4Cl, 2 mM $MgSO_4$, 0.1 mM $CaCl_2$, A5 trace metals mix (2.86 mg l^{-1} H_3BO_3, 1.81

mg l^{-1} $MnCl_2 \cdot 4H_2O$, 0.079 mg l^{-1} $CuSO_4 \cdot 5H_2O$, 49.4 µg l^{-1} $Co(NO_3)_2 \cdot 6H_2O$, 0.22 g l^{-1} $ZnSO_4.7H_2O$, 0.39 g l^{-1} $Na_2MoO_4.2H_2O$), varying concentrations of glucose, and appropriate antibiotics. M9P medium consists of M9 minimal medium supplemented with 5 g L^{-1} of yeast extract and appropriate antibiotics. M9YT medium consists of M9 minimal medium supplemented with 6 g L^{-1} casein digest peptone, 12 g L^{-1} yeast extract, and appropriate antibiotics. The inducer used was isopropyl-β-D-1-thiogalactopyranoside (IPTG) at 1 mM. The optical density at 600 nm (OD_{600}) was measured with a Synergy H1 hybrid plate reader (BioTek Instruments, Inc.).

2.4. D-glucosamine and D-sedoheptulose production experiments

For regular cell density production experiments, overnight cultures were inoculated at 1% into 3 mL of M9P medium or M9YT medium as described. Cells were grown at 37 °C until the OD_{600} described, then induced with 1 mM IPTG if necessary, and grown at 30 °C for 24 h.

2.5. Sugar Quantification

Analysis of D-glucose, D-glucosamine and D-sedoheptulose concentrations was performed using High-Performance Anion-Exchange (HPAE) with Pulsed Amperometric Detection (PAD) on an ICS-5000+ system with a CarboPac PA20 3x150mm (Thermo Fisher) and Dionex™ AminoTrap Column (Thermo Fisher). The equilibrium phase was comprised of 50 mM NaOH in degassed MilliQ water at a flow rate of 0.3 mL min^{-1} for 10 min. Mobile phase was comprised of 50 mM NaOH in degassed MilliQ water at a flow rate of 0.3 mL min^{-1} for 20 min. Mobile phase was changed to 200 mM NaOH from min 20-50 min. The column oven was maintained at 30 °C.

To prepare samples for HPAE-PAD analysis, 300 uL of culture was centrifuged at 17,000 g for 3 min. Supernatants were diluted 250-fold and applied to a 0.2 mm PVDF hydrophilic membrane 96 well filter plate and centrifuged at 2,000 g for 5 min into a polystyrene 96 well. Sugar concentrations were determined using external calibration curves prepared from authentic standards.

2.6. Structure Prediction

Full-length GlmS monomer structures (609 residues) were predicted for wild-type, GlmS54 (A38T, R249C, G471S), and GlmS* (A38T, R249C) using ColabFold v1.5 (Mirdita et al., 2022) with AlphaFold2 (Jumper et al., 2021). Multiple sequence alignments were generated using MMseqs2 against the ColabFold database. Five models were generated per variant using AlphaFold2-multimer-v3 weights with 3 recycles, followed by AMBER force field relaxation. The top-ranked model for each variant (by pLDDT) was selected for downstream analysis. Model quality was assessed by mean pLDDT and pTM scores.

2.7. Rosetta Cartesian ΔΔG Calculations

The effect of each mutation on protein thermodynamic stability was assessed using the Rosetta Cartesian ΔΔG protocol (Park et al., 2016). The best ColabFold model for wild-type GlmS was first refined using Rosetta FastRelax (Conway et al., 2014) with coordinate constraints (ref2015 score function, 500 independent trajectories), and the lowest-energy structure was selected as the reference. Cartesian ΔΔG calculations were performed using the ref2015_cart score function with 3 iterations per mutation. Individual ΔΔG values were computed for A38T, R249C, and G471S, as well as combined ΔΔG values for the double mutant (A38T/R249C) and triple mutant

(A38T/R249C/G471S). Mutation files specified the wild-type and mutant residue identities at each position, and combined variants included all constituent mutations simultaneously. Stability effects were interpreted following the guidelines of Kellogg et al. (2011), where ΔΔG values < 5 REU are considered tolerable for protein function.

2.8. Protein–Ligand Complex Modeling

Structures of each GlmS variant in complex with GlcN-6-P were predicted using Boltz-2 (Passaro et al., 2025). Input files specified the full-length protein sequence and the GlcN-6-P ligand as a SMILES string (N[C@H]1C(O)O[C@H](COP(=O)(O)O)[C@@H](O)[C@@H]1O). Both monomer (single chain + ligand) and homodimer (two identical chains + ligand per chain) complexes were modeled. Multiple sequence alignments were generated using the ColabFold MSA server. Structure prediction used the default Boltz-2 model with one sample per input. Prediction confidence was assessed by the Boltz-2 confidence score, ligand ipTM, and protein ipTM. Ligand binding pose analysis was performed by measuring minimum interatomic distances between ligand heavy atoms and protein residue heavy atoms using BioPython (Cock et al., 2009). Mutation-to-ligand distances were measured in the same manner. Predicted aligned error (PAE) values for the protein-ligand interface were extracted from the Boltz-2 output.

2.9. Statistical analysis

Data are presented as mean ± standard deviation from three biological replicates. Statistical analyses were performed using one-way analysis of variance (ANOVA) followed by Dunnett's multiple comparisons test (two-sided). Statistical significance was defined as $P \leq 0.05$.

3. Results and Discussion

3.1. Native D-glucosamine production capability of *E. coli*

In prior work, AL4731 (Δ*pfkA* Δ*zwf* Δ*alsE* Δ*manA* Δ*pgm* Δ*gatZ* Δ*mtlD* **Table 1**) was developed to redirect carbon flux away from dominant glucose utilization pathways and competing sugar products and was shown to accumulate D-sedoheptulose (Palur et al., 2025). Upon re-examination of this strain grown on D-glucose, we detected accumulation of D-glucosamine in addition to the expected D-sedoheptulose production (**Fig. 2a**). AL4731 (**Table 1**) accumulated 0.2 g L^{-1} D-glucosamine alongside 0.75 g L^{-1} D-sedoheptulose (**Fig. 2a**). The accumulation of D-glucosamine in the absence of heterologous enzymes demonstrates that *E. coli* natively possesses the enzymatic capacity to convert D-glucose to D-glucosamine. These results further demonstrate that systematic elimination of competing carbon sinks can reveal latent biosynthetic activities that are normally masked by dominant metabolic pathways.

3.2. Screening of phosphatases for D-glucosamine and D-sedoheptulose production

We hypothesized that endogenous F6P is aminated to GlcN6P by GlmS, coupled to glutamine conversion to glutamate (Teplyakov et al., 2002), and that accumulation of D-glucosamine requires subsequent dephosphorylation of GlcN-6P (**Fig. 1**). While the amination step catalyzed by GlmS is well established, the identity of native phosphatases capable of efficiently converting GlcN6P to D-glucosamine is not obvious and represents a critical unresolved step for endogenous amino sugar production. To address this limitation, we selected a panel of promiscuous phosphatases (Kuznetsova et al., 2006) and screened hexitol phosphatase B (HxpB), sugar phosphatase YbiV,

sugar phosphatase YidA, hexitol phosphatase A (HxpA), α-D-glucose-1-phosphate phosphatase YihX, phosphosugar phosphatase YigL, and fructose-1-phosphate phosphatase YqaB by co-expressing each gene with *glmS* (pAL2937–pAL2943; **Table 2**) in strain AL4731 (Δ*pfkA* Δ*zwf* Δ*alsE* Δ*manA* Δ*pgm* Δ*gatZ* Δ*mtlD,* **Table 1**). In most cases, this modification selectively increased D-sedoheptulose production without enhancing D-glucosamine accumulation (**Fig. 2a**). Given their broad substrate specificity, overexpression of these phosphatase genes may also affect cellular physiology through activity toward other intracellular phosphorylated metabolites, and such effects may contribute to differences in growth and production phenotypes (**Fig. 2**). This outcome is consistent with feedback inhibition of GlmS by GlcN6P, whereby inefficient dephosphorylation leads to intracellular GlcN6P buildup, suppressing further amination of F6P and limiting flux toward D-glucosamine. These results indicate that phosphatase activity alone is insufficient to enhance D-glucosamine production when GlmS remains subject to product inhibition and highlight phosphatase identity as a key control point governing carbon flux distribution.

Previous studies have shown that mutations in GlmS, namely GlmS54 (A38T, R249C, G471S), can relieve feedback inhibition by GlcN6P (Deng et al., 2006a). Based on this, we next replaced wild-type *glmS* with *glmS54* and co-expressed the same set of native phosphatases (pAL2906, pAL2907, pAL2908, pAL2909, pAL2910, pAL2911, pAL2912, **Table 2**) in AL4731 (Δ*pfkA* Δ*zwf* Δ*alsE* Δ*manA* Δ*pgm* Δ*gatZ* Δ*mtlD,* **Table 1**). In contrast to the wild-type enzyme, expression of *glmS54* resulted in substantially increased D-glucosamine accumulation across multiple phosphatase backgrounds (**Fig. 2b**), indicating relief of feedback inhibition by GlcN6P and increased flux through the

GlmS-catalyzed amination reaction (Deng et al., 2006a). Strikingly, the relative distribution between D-glucosamine and D-sedoheptulose varied with the identity of the co-expressed phosphatase, demonstrating that phosphatase substrate preference functions as a dominant determinant of metabolic flux partitioning. Among the phosphatases evaluated, additional expression of *ybiV* uniquely directed carbon flux toward exclusive D-glucosamine production, yielding 3.07 g L^{-1} D-glucosamine with no detectable D-sedoheptulose formation (**Fig. 2b**). In contrast, all other phosphatases supported varying degrees of D-sedoheptulose formation. This result identifies YbiV as a selective phosphatase for endogenous D-glucosamine biosynthesis and establishes phosphatase identity as a powerful control point for directing product specificity within the platform.

3.3. Increased glucose uptake via alternate glucose transporter

In *E. coli*, accumulation of intracellular sugar phosphates induces glucose-phosphate stress and suppresses glucose uptake through destabilization of *ptsG* mRNA, which encodes the glucose-specific PTS transporter (Kessler et al., 2017; Morita et al., 2003). To alleviate this limitation, we additionally expressed *galP*, encoding a galactose-proton symporter (Macpherson et al., 1983), together with *glk*, encoding glucokinase (pAL2264, **Table 2**). These modifications enable PTS-independent glucose uptake via GalP and subsequent phosphorylation to glucose-6-phosphate by Glk (Meyer et al., 1997).

Although this modification increased glucose uptake, it selectively enhanced D-sedoheptulose production while reducing D-glucosamine titers, indicating that the increased carbon flux was preferentially diverted toward D-sedoheptulose formation

rather than amino sugar biosynthesis (**Fig. 3**). These results indicate that glucose uptake is not the primary constraint on D-glucosamine production under these conditions and that simply increasing carbon influx does not enhance flux through the GlmS-dependent pathway. In addition, all further experiments employed YbiV as the phosphatase to maintain selective D-glucosamine production.

3.4. Eliminating futile cycling to enhance D-glucosamine production

In *E. coli*, NagB (GlcN6P deaminase) catalyzes the reverse of the GlmS reaction, converting GlcN6P back to F6P with concomitant release of ammonia (White and Pasternak, 1967), thereby directly opposing net D-glucosamine biosynthesis (**Fig. 1**). To eliminate this futile cycling and stabilize flux toward amino sugar formation, we deleted *nagB* in AL4731, generating strain AL4974 (Δ*pfkA* Δ*zwf* Δ*alsE* Δ*manA* Δ*pgm* Δ*gatZ* Δ*mtlD* Δ*nagB*, **Table 1**). When *glmS54* and *ybiV* were co-expressed (pAL2908; **Table 2**) in this background, D-glucosamine production increased further, reaching 3.52 g L^{-1} (**Fig. 4**). These results demonstrate that removal of the NagB-mediated reverse reaction is an effective strategy to reinforce forward flux through the endogenous glucosamine biosynthetic pathway and improve overall D-glucosamine accumulation.

During strain construction and screening, we observed that certain colonies consistently outperformed others despite having identical intended genotypes. Sequencing of the plasmid isolated from these high-performing strains revealed a modified *glmS* containing two amino acid substitutions (A38T, R249C; pAL3004, **Table 2**) relative to GlmS54. While prior studies have characterized the functional impact of each individual mutation present in GlmS54, the combined contribution of all three substitutions has not been directly compared with intermediate mutant variants (Deng et

al., 2006a). Expression of the double-mutant GlmS* (A38T, R249C) gene produced 4.01 g L^{-1} D-glucosamine, which was not significantly different from that obtained with GlmS54 (**Fig. 4**). This observation indicates that the A38T and R249C substitutions are sufficient to reproduce the enhanced production phenotype associated with GlmS54 under the conditions examined here. Consequently, all subsequent experiments employed the double-mutant GlmS* variant. While G471S has been reported to influence GlmS activity when evaluated individually (Deng et al., 2006a), our results suggest that this substitution is not required to achieve improved D-glucosamine production in the presence of A38T and R249C.

3.5. Structural and thermodynamic analysis of GlmS variants

Feedback-insensitive variants of GlmS have previously been identified through directed evolution, including the triple mutant GlmS54 (A38T, R249C, G471S), which exhibits reduced sensitivity to product inhibition by GlcN-6-P and enhanced glucosamine production (Deng et al., 2006a). Specifically, GlmS54 displays a Ki for GlcN-6-P of 2.5 mM compared to 0.56 mM for the wild-type enzyme (Deng et al., 2006a). However, mapping these substitutions onto the crystal structure of the GlmS isomerase domain (PDB: 1MOQ) (Teplyakov et al., 1998) revealed that all three mutated residues are located more than 16 Å from the GlcN-6-P binding site, providing no obvious structural explanation for the reduced product inhibition.

We identified a double mutant GlmS* (A38T, R249C) that performed comparably to the triple mutant GlmS54 in D-glucosamine production (**Fig. 4**), suggesting that the G471S substitution does not substantially contribute to the improved phenotype under our experimental conditions. To determine whether the similar performance of GlmS

and GlmS54 could be associated with readily apparent structural differences, we compared computational models of the wild-type and variant GlmS proteins. Full-length GlmS structures for the wild-type enzyme, GlmS54 (A38T, R249C, G471S), and GlmS* (A38T, R249C) were predicted using LocalColabFold (Mirdita et al., 2022) with AlphaFold2 (Jumper et al., 2021), followed by AMBER relaxation. All models were generated with high confidence, with mean pLDDT scores ranging from 92.5 to 92.8. Structural superposition revealed highly similar overall conformations across all variants, with no apparent structural rearrangements at or proximal to the mutation sites.

To quantitatively assess the impact of each mutation on protein thermodynamic stability, Rosetta Cartesian ΔΔG calculations were performed using the ref2015_cart score function (Park et al., 2016). The lowest-energy relaxed wild-type structure was used as the reference state. All mutations were predicted to be neutral to mildly destabilizing (**Tables S4** and **S5**). The calculated cumulative ΔΔG for the double mutant (+1.7 REU) was lower than that of the triple mutant (+4.9 REU), indicating that the G471S substitution introduces an additional stability penalty. Given that both values fall within the range generally considered compatible with preserved protein function (ΔΔG < 5 REU) (Kellogg et al., 2011), these results suggest that the mutations do not substantially compromise overall structural integrity. Thus, the computational analyses did not identify an apparent structural or thermodynamic feature that would explain an additional contribution of G471S under the conditions examined.

To determine whether the mutations influence the GlcN-6-P binding site or alter ligand interaction geometry, structures of each variant in complex with GlcN-6-P were

predicted using Boltz-2 (Passaro et al., 2025). Both monomeric and homodimeric complexes were modeled for the wild-type enzyme, GlmS54, and GlmS*. In all cases, GlcN-6-P was predicted to occupy the same active-site pocket, engaging an identical set of interacting residues (Thr353, Ser304, Gln349, Ser350, and Thr303), each located within 2.5–2.8 Å of the ligand (**Fig. S1**). The mutation sites were spatially distant from the bound product: A38 is approximately 38 Å from the nearest ligand atom, whereas R249C and G471S are approximately 18 Å and 19 Å away, respectively, within the same protomer. These structural predictions indicate that the substitutions do not directly perturb the active site or product-binding interactions.

Collectively, these computational analyses indicate that the A38T, R249C, and G471S substitutions do not alter the global fold of GlmS, substantially compromise thermodynamic stability, or modify the geometry of the GlcN-6-P binding pocket. The predicted structures are virtually superimposable in the active-site region across all variants. All three mutation sites are located on the solvent-exposed surface of the enzyme and are spatially distant from the ligand-binding pocket (**Fig. S1**): A38 is approximately 38 Å from the nearest ligand atom, R249 approximately 18 Å, and G471 approximately 19 Å. Rosetta Cartesian ΔΔG calculations predicted each substitution to be neutral to mildly destabilizing (A38T: +0.0 REU; R249C: +2.7 REU; G471S: +2.8 REU), with cumulative ΔΔG values of +1.7 REU for the double mutant GlmS* and +4.9 REU for the triple mutant GlmS54, both within the range generally compatible with preserved protein function. These findings are consistent with previous structural analyses showing that the mutated residues lie more than 16 Å from the active site (Deng et al., 2006a).

While these computational analyses provide a consistent structural and thermodynamic framework for interpreting the effects of the GlmS mutations, they are not directly validated by experimental measurements of protein structure or dynamics. Therefore, the conclusions drawn here should be considered as hypotheses that complement the observed phenotypic data rather than definitive mechanistic explanations. In particular, potential effects on conformational dynamics, allosteric communication, or catalytic kinetics cannot be resolved by static structure prediction and require further experimental investigation.

3.6. Reducing glucosamine assimilation

To further minimize product loss through reuptake, we next targeted native glucosamine assimilation pathways in *E. coli*. Glucosamine is primarily imported via the NagE PTS transporter (John Rogers et al., 1988) and, to a lesser extent, through the mannose-family PTS encoded by ManXYZ (Erni and Zanolari, 1985). To reduce glucosamine uptake during production, we constructed strains carrying deletions of *nagE* in AL4974, resulting in AL4959 (Δ*pfkA* Δ*zwf* Δ*alsE* Δ*manA* Δ*pgm* Δ*gatZ* Δ*mtlD* Δ*nagB* Δ*nagE*, **Table 1**) and *manXYZ*, resulting in AL4980 (Δ*pfkA* Δ*zwf* Δ*alsE* Δ*manA* Δ*pgm* Δ*gatZ* Δ*mtlD* Δ*nagB* Δ*nagE* Δ*manXYZ*, **Table 1**). In both strains, glucosamine consumption remained largely unchanged after 24 h, suggesting that additional transport systems may contribute to glucosamine uptake under these conditions (**Fig. S2a**).

When these transporter-deficient strains (AL4959 and AL4980, **Table 1**) were evaluated under D-glucosamine production conditions with the production plasmid pAL3004 (*PgadB:glmS**(A38T, R249C)–*ybiV*, **Table 2**), both deletions resulted in

reduced D-glucosamine production relative to the parent strain (**Fig. S2b**). Thus, although *nagE* and *manXYZ* were targeted to reduce D-glucosamine reuptake, disruption of these transport systems did not improve extracellular D-glucosamine accumulation and instead negatively affected production under the conditions examined. The physiological basis for this effect remains unclear, as PTS transport systems can influence broader cellular metabolic and regulatory functions beyond substrate uptake (Commichau et al., 2006; Doucette et al., 2011; Västermark and Saier, 2014). Based on these results, subsequent engineering efforts were conducted using AL4974 (Δ*pfkA* Δ*zwf* Δ*alsE* Δ*manA* Δ*pgm* Δ*gatZ* Δ*mtlD* Δ*nagB*, **Table 1**).

3.7. Modulating ammonia assimilation to increase glutamine availability

In *E. coli*, intracellular glutamine levels are tightly controlled by the glutamine synthetase–glutamate synthase (GS–GOGAT) cycle, which serves as the primary route for ammonia assimilation under both nitrogen-limited and nitrogen-replete conditions (Miyakoshi, 2024). GS, encoded by *glnA*, catalyzes the ATP-dependent conversion of glutamate and ammonia to glutamine (Niranda-Rjos et al., 1987), while GOGAT, encoded by *gltBD*, transfers the amide nitrogen of glutamine to α-ketoglutarate to regenerate glutamate (**Fig. 1**) (Goss et al., 2001). Flux through this cycle is stringently regulated through covalent adenylylation of GS by the bifunctional adenylyltransferase/adenylyl-removing enzyme GlnE and by transcriptional control mediated by the Ntr regulatory system, thereby preventing excessive glutamine accumulation (Miyakoshi, 2024; Reitzer, 2003).

To increase intracellular glutamine availability for the GlmS-catalyzed amination step, we systematically disrupted key regulatory and consumption nodes within the GS–

GOGAT network. First, deletion of *glnE* in AL4974 (**Table 1**) was expected to reduce GS adenylylation and promote glutamine synthesis, yielding strain AL5035 (Δ*pfkA* Δ*zwf* Δ*alsE* Δ*manA* Δ*pgm* Δ*gatZ* Δ*mtlD* Δ*nagB* Δ*glnE*, **Table 1**). To further reduce glutamine consumption, *gltBD* was deleted to block glutamine-dependent glutamate regeneration, generating AL5038 (Δ*pfkA* Δ*zwf* Δ*alsE* Δ*manA* Δ*pgm* Δ*gatZ* Δ*mtlD* Δ*nagB* Δ*gltBD*, **Table 1**). Combined deletion of *glnE* and *gltBD* produced AL5039 (Δ*pfkA* Δ*zwf* Δ*alsE* Δ*manA* Δ*pgm* Δ*gatZ* Δ*mtlD* Δ*nagB* Δ*glnE* Δ*gltBD*, **Table 1**). In addition, the production medium was supplemented with tryptone to provide readily assimilable amino acids and peptides that could contribute directly to intracellular glutamine pools.

AL4974, AL5035, AL5038, and AL5039 harboring pAL3004 and pAL2264 (**Table 2**) produced 4.5, 5.2, 4.7, and 5.5 g L^{-1} D-glucosamine, respectively (**Fig. 5**). Disruption of the GS–GOGAT system resulted in modest increases in D-glucosamine production. The relatively small improvements suggest that glutamine availability is only one of several factors influencing flux through the GlmS-catalyzed reaction and that additional regulatory constraints remain (Woolfolk and Stadtman, 1967). Nevertheless, the highest titers were observed in AL5039 (Δ*glnE* Δ*gltBD*, **Table 1**), indicating that simultaneous relief of GS regulation and suppression of glutamine consumption provide additive benefits for D-glucosamine production.

3.8. Enhancing nitrogen assimilation capacity to support D-glucosamine biosynthesis

Because glutamine serves as the direct nitrogen donor for the GlmS-catalyzed conversion of F6P to GlcN6P, we next sought to increase intracellular glutamine availability by additionally expressing *glnA*, which encodes GS (Niranda-Rjos et al.,

1987). GS catalyzes the ATP-dependent assimilation of ammonia into glutamate to form glutamine and constitutes the primary entry point of inorganic nitrogen into cellular metabolism (**Fig. 1**) (Miyakoshi, 2024). Under native conditions, GS activity is stringently regulated at both transcriptional and post-translational levels to maintain low steady-state glutamine pools, thereby constraining flux through glutamine-dependent biosynthetic reactions (Woolfolk and Stadtman, 1967). We therefore hypothesized that direct amplification of GS expression would increase glutamine biosynthetic capacity and enhance D-glucosamine production through the GlmS-catalyzed reaction. Consistent with this hypothesis, additional expression of *glnA* had a positive effect on D-glucosamine production across all strain backgrounds tested (**Fig. 5b**). The highest D-glucosamine titer of 9.2 g L^{-1} was obtained with AL5035 harboring pAL3004 and pAL2920 (**Fig. 5b**). Co-expression of *glnA* (pAL2920, **Table 2**) with the glucosamine production plasmid (pAL3004, **Table 2**) increased D-glucosamine production (**Fig. 5b**). In contrast, deletion of *glnE* or *gltBD* alone yielded only modest improvements (**Fig. 5a**). Together, these results demonstrate that increasing glutamine biosynthetic capacity through additional expression of *glnA* can enhance D-glucosamine production and identify glutamine biosynthesis as an important metabolic control point in this production system.

In parallel, we examined whether additional nitrogen supplementation at the medium level could further enhance D-glucosamine production. To probe potential nitrogen limitation under both medium backgrounds, urea, ammonium chloride, and L-glutamine were supplemented at concentrations of 1, 2, 5, and 10 g L^{-1} (**Fig. 6**). Urea was evaluated as a slowly metabolized nitrogen source capable of sustaining

intracellular ammonia availability (Mobley and Hausinger, 1989), ammonium chloride as a readily assimilable inorganic nitrogen source directly supporting glutamine synthetase activity (Vo et al., 2013), and L-glutamine as an organic nitrogen source and immediate precursor for glucosamine biosynthesis. Across all tested conditions, supplementation with these nitrogen sources did not further increase D-glucosamine titers (**Fig. 6**). These results indicate that complex nitrogen sources already provide sufficient assimilable nitrogen to support glucosamine biosynthesis and that further increasing extracellular nitrogen availability does not confer additional benefit under these conditions.

4. Concluding Remarks

This study establishes *E. coli* as a viable platform for D-glucosamine production by revealing and exploiting a native metabolic route that connects central carbon metabolism to amino sugar biosynthesis. We show that increasing glucose uptake alone does not enhance D-glucosamine production, whereas modulation of nitrogen metabolism, particularly glutamine biosynthesis, can substantially improve production.

By combining a feedback-insensitive GlmS variant with selective endogenous phosphatase activity, we demonstrate tunable flux partitioning between D-glucosamine and D-sedoheptulose, with YbiV enabling selective D-glucosamine production. Removal of futile reactions and targeted enhancement of glutamine biosynthesis further improved production, highlighting the importance of coordinating carbon and nitrogen metabolism.

Overall, this work demonstrates that amplification and redirection of endogenous metabolic capacity, rather than heterologous pathway engineering, provides an effective strategy for microbial D-glucosamine production. Beyond establishing a genetically defined D-glucosamine production pathway and strain platform, this study identifies key

metabolic control points governing amino sugar biosynthesis, providing a foundation for future optimization under industrially relevant cultivation conditions. Further improvement in D-glucosamine titer will require both continued strain engineering and optimization of cultivation conditions, particularly given the chemical instability of D-glucosamine in cultivation media. Evaluation of industrial performance will require bioreactor studies under application-specific process conditions, including medium formulation, substrate selection, and feeding strategies. Because the objective of this work was pathway discovery and strain development, such process optimization was beyond the scope of the present study.

An advantage of this strategy is that D-glucosamine production is achieved by redirecting endogenous *E. coli* metabolism rather than introducing a heterologous biosynthetic pathway, while phosphatase selection provides control over product specificity. A current limitation is that production performance has been evaluated under small-scale cultivation conditions designed primarily for pathway construction and strain development. Further strain engineering and optimization under application-relevant cultivation conditions will be important for evaluating and improving the production potential of this platform.

Author contributions

D.P., A.B., B.L, J.D., J.S., and S.A. designed research; D.P., A.B., and B.L. performed the experiments; D.P., A.B., B.L., I.A., J.S., and S.A. analyzed data; D.P., A.B., B.L, I.A., J.D., J.S., and S.A. wrote the manuscript.

Declaration of competing interests

The authors declare the following financial interests which may be considered as potential competing interests: Dileep Sai Kumar Palur, Amey Bait, Bryant Luu, Ian C. Anderson, Justin B. Siegel, and Shota Atsumi are inventors on the patent application related to this study. John Didzbalis is an employee of Mars, Incorporated, a manufacturer of food and confectionery.

Data availability

The datasets generated in this study are available from the corresponding author on reasonable request.

Acknowledgements

This work was supported by Mars, Incorporated.

Reference

Ahuja, V., Bhatt, A.K., Sharma, V., Rathour, R.K., Rana, N., Bhatia, R.K., Varjani, S., Kumar, M., Magdouli, S., Yung-HunYang, Bhatia, S.K., 2025. Advances in glucosamine production from waste biomass and microbial fermentation technology and its applications. Biomass Convers. Biorefinery 15, 1643–1665. https://doi.org/10.1007/s13399-021-01968-y

Baba, T., Ara, T., Hasegawa, M., Takai, Y., Okumura, Y., Baba, M., Datsenko, K.A., Tomita, M., Wanner, B.L., Mori, H., 2006. Construction of *Escherichia coli* K-12 in-frame, single-gene knockout mutants: the Keio collection. Mol. Syst. Biol. 2, 2006.0008. https://doi.org/10.1038/msb4100050

Bertuzzi, D.L., Becher, T.B., Capreti, N.M.R., Amorim, J., Jurberg, I.D., Megiatto, J.D., Ornelas, C., 2018. General Protocol to Obtain D-Glucosamine from Biomass Residues: Shrimp Shells, Cicada Sloughs and Cockroaches. Glob. Chall. 2, 1800046. https://doi.org/10.1002/gch2.201800046

Bhathal, A., Spryszak, M., Louizos, C., Frankel, G., 2017. Glucosamine and chondroitin use in canines for osteoarthritis: A review. Open Vet. J. 7, 36–49. https://doi.org/10.4314/ovj.v7i1.6

Bordegé, V., Muñoz-Bonilla, A., León, O., Sánchez-Chaves, M., Cuervo-Rodríguez, R., Fernández-García, M., 2011. Glycopolymers with glucosamine pendant groups: Copolymerization, physico-chemical and interaction properties. React. Funct. Polym. 71, 1–10. https://doi.org/10.1016/j.reactfunctpolym.2010.11.010

Chen, X., Liu, L., Li, J., Du, G., Chen, J., 2012. Improved glucosamine and N-acetylglucosamine production by an engineered *Escherichia coli* via step-wise regulation of dissolved oxygen level. Bioresour. Technol. 110, 534–538. https://doi.org/10.1016/j.biortech.2011.12.015

Cock, P.J.A., Antao, T., Chang, J.T., Chapman, B.A., Cox, C.J., Dalke, A., Friedberg, I., Hamelryck, T., Kauff, F., Wilczynski, B., de Hoon, M.J.L., 2009. Biopython: freely available Python tools for computational molecular biology and bioinformatics. Bioinformatics 25, 1422–1423. https://doi.org/10.1093/bioinformatics/btp163

Commichau, F.M., Forchhammer, K., Stülke, J., 2006. Regulatory links between carbon and nitrogen metabolism. Curr. Opin. Microbiol., Cell Regulation / Edited by Werner Goebel and Stephen Lory 9, 167–172. https://doi.org/10.1016/j.mib.2006.01.001

Conway, P., Tyka, M.D., DiMaio, F., Konerding, D.E., Baker, D., 2014. Relaxation of backbone bond geometry improves protein energy landscape modeling. Protein Sci. Publ. Protein Soc. 23, 47–55. https://doi.org/10.1002/pro.2389

Cowan, A.E., Klass, S.H., Winegar, P.H., Keasling, J.D., 2023. Microbial production of fuels, commodity chemicals, and materials from sustainable sources of carbon and energy. Curr. Opin. Syst. Biol. 36, 100482. https://doi.org/10.1016/j.coisb.2023.100482

Deng, M.-D., Grund, A.D., Wassink, S.L., Peng, S.S., Nielsen, K.L., Huckins, B.D., Walsh, B.L., Burlingame, R.P., 2006a. Directed evolution and characterization of *Escherichia coli* glucosamine synthase. Biochimie 88, 419–429. https://doi.org/10.1016/j.biochi.2005.10.002

576 Deng, M.-D., Severson, D.K., Grund, A.D., Wassink, S.L., Burlingame, R.P., Berry, A.,
577 Running, J.A., Kunesh, C.A., Song, L., Jerrell, T.A., Rosson, R.A., 2005. Metabolic
578 engineering of *Escherichia coli* for industrial production of glucosamine and N-
579 acetylglucosamine. Metab. Eng. 7, 201–214.
580 https://doi.org/10.1016/j.ymben.2005.02.001
581 Deng, M.-D., Wassink, S.L., Grund, A.D., 2006b. Engineering a new pathway for N-
582 acetylglucosamine production: Coupling a catabolic enzyme, glucosamine-6-
583 phosphate deaminase, with a biosynthetic enzyme, glucosamine-6-phosphate N-
584 acetyltransferase. Enzyme Microb. Technol. 39, 828–834.
585 https://doi.org/10.1016/j.enzmictec.2006.01.008
586 Doucette, C.D., Schwab, D.J., Wingreen, N.S., Rabinowitz, J.D., 2011. α-ketoglutarate
587 coordinates carbon and nitrogen utilization via Enzyme I inhibition. Nat. Chem. Biol.
588 7, 894–901. https://doi.org/10.1038/nchembio.685
589 Erni, B., Zanolari, B., 1985. The mannose-permease of the bacterial phosphotransferase
590 system. Gene cloning and purification of the enzyme IIMan/IIIMan complex of
591 *Escherichia coli*. J. Biol. Chem. 260, 15495–15503. https://doi.org/10.1016/S0021-
592 9258(17)36282-8
593 Gao, K., Qin, Y., Liu, S., Wang, L., Xing, R., Yu, H., Chen, X., Li, P., 2023. A review of the
594 preparation, derivatization and functions of glucosamine and *N*-acetyl-glucosamine
595 from chitin. Carbohydr. Polym. Technol. Appl. 5, 100296.
596 https://doi.org/10.1016/j.carpta.2023.100296
597 Glucosamine Market Size [WWW Document], 2025. URL
598 https://www.precedenceresearch.com/glucosamine-market.
599 Goss, T.J., Perez-Matos, A., Bender, R.A., 2001. Roles of Glutamate Synthase, gltBD, and
600 gltF in Nitrogen Metabolism of *Escherichia coli* and *Klebsiella aerogenes*. J.
601 Bacteriol. 183, 6607–6619. https://doi.org/10.1128/JB.183.22.6607-6619.2001
602 Guan, Z.-B., Deng, X.-T., Zhang, Z.-H., Xu, G.-C., Cheng, W.-L., Liao, X.-R., Cai, Y.-J., 2024.
603 Engineering Glucosamine-6-Phosphate Synthase to Achieve Efficient One-Step

Biosynthesis of Glucosamine. ACS Chem. Biol. 19, 1237–1242. https://doi.org/10.1021/acschembio.4c00144

Hong, P.K., Betti, M., 2016. Non-enzymatic browning reaction of glucosamine at mild conditions: Relationship between colour formation, radical scavenging activity and α-dicarbonyl compounds production. Food Chem. 212, 234–243. https://doi.org/10.1016/j.foodchem.2016.05.170

Hsieh, J.-W., Wu, H.-S., Wei, Y.-H., Wang, S.S., 2007. Determination and Kinetics of Producing Glucosamine Using Fungi. Biotechnol. Prog. 23, 1009–1016. https://doi.org/10.1021/bp070037o

Jiang, Y., Chen, B., Duan, C., Sun, B., Yang, J., Yang, S., 2015. Multigene Editing in the Escherichia coli Genome via the CRISPR-Cas9 System. Appl. Environ. Microbiol. 81, 2506–2514. https://doi.org/10.1128/AEM.04023-14

John Rogers, M., Ohgi, T., Plumbridge, J., Söil, D., 1988. Nucleotide sequences of the Escherichia coli nagE and nagB genes: the structural genes for the N-acetylglucosamine transport protein of the bacterial phosphoenolpyruvate: sugar phosphotrans-ferase system and for glucosamine-6-phosphate deaminase. Gene 62, 197–207. https://doi.org/10.1016/0378-1119(88)90558-6

Jumper, J., Evans, R., Pritzel, A., Green, T., Figurnov, M., Ronneberger, O., Tunyasuvunakool, K., Bates, R., Žídek, A., Potapenko, A., Bridgland, A., Meyer, C., Kohl, S.A.A., Ballard, A.J., Cowie, A., Romera-Paredes, B., Nikolov, S., Jain, R., Adler, J., Back, T., Petersen, S., Reiman, D., Clancy, E., Zielinski, M., Steinegger, M., Pacholska, M., Berghammer, T., Bodenstein, S., Silver, D., Vinyals, O., Senior, A.W., Kavukcuoglu, K., Kohli, P., Hassabis, D., 2021. Highly accurate protein structure prediction with AlphaFold. Nature 596, 583–589. https://doi.org/10.1038/s41586-021-03819-2

Kang, H.E., Kim, S.J., Yeo, E., Hong, J., Rajgopal, A., Hu, C., Murray, M.A., Dang, J., Park, E., 2022. Pharmacokinetic Comparison of Chitosan-Derived and Biofermentation-Derived Glucosamine in Nutritional Supplement for Bone Health. Nutrients 14, 3213. https://doi.org/10.3390/nu14153213

Kellogg, E.H., Leaver-Fay, A., Baker, D., 2011. Role of conformational sampling in computing mutation-induced changes in protein structure and stability. Proteins 79, 830–838. https://doi.org/10.1002/prot.22921

Kessler, J.R., Cobe, B.L., Richards, G.R., 2017. Stringent Response Regulators Contribute to Recovery from Glucose Phosphate Stress in Escherichia coli. Appl. Environ. Microbiol. 83, e01636-17. https://doi.org/10.1128/AEM.01636-17

Kuznetsova, E., Proudfoot, M., Gonzalez, C.F., Brown, G., Omelchenko, M.V., Borozan, I., Carmel, L., Wolf, Y.I., Mori, H., Savchenko, A.V., Arrowsmith, C.H., Koonin, E.V., Edwards, A.M., Yakunin, A.F., 2006. Genome-wide Analysis of Substrate Specificities of the Escherichia coli Haloacid Dehalogenase-like Phosphatase Family *. J. Biol. Chem. 281, 36149–36161. https://doi.org/10.1074/jbc.M605449200

Li, M.Z., Elledge, S.J., 2007. Harnessing homologous recombination in vitro to generate recombinant DNA via SLIC. Nat. Methods 4, 251–256. https://doi.org/10.1038/nmeth1010

Li, P., Li, X., Wen, Z., Dong, R., Li, K., Fan, H., Wang, R., Wang, J., Lv, M., 2020. Enhancement of Production of d-Glucosamine in Escherichia coli by Blocking Three Pathways Involved in the Consumption of GlcN and GlcNAc. Mol. Biotechnol. 62, 387–399. https://doi.org/10.1007/s12033-020-00257-9

Luu, B., Palur, D.S.K., Taylor, J.E., Didzbalis, J., Siegel, J.B., Atsumi, S., 2025. Unleashing the innate ability of Escherichia coli to produce D-Allose. Metab. Eng. 88, 206–214. https://doi.org/10.1016/j.ymben.2025.01.007

Macpherson, A.J., Jones-Mortimer, M.C., Horne, P., Henderson, P.J., 1983. Identification of the GalP galactose transport protein of Escherichia coli. J. Biol. Chem. 258, 4390–4396. https://doi.org/10.1016/S0021-9258(18)32635-8

Meng, D., Wei, X., Bai, X., Zhou, W., You, C., 2020. Artificial in Vitro Synthetic Enzymatic Biosystem for the One-Pot Sustainable Biomanufacturing of Glucosamine from Starch and Inorganic Ammonia. ACS Catal. 10, 13809–13819. https://doi.org/10.1021/acscatal.0c03767

Mengin-Lecreulx, D., van Heijenoort, J., 1994. Copurification of glucosamine-1-phosphate acetyltransferase and N-acetylglucosamine-1-phosphate uridyltransferase activities of Escherichia coli: characterization of the glmU gene product as a bifunctional enzyme catalyzing two subsequent steps in the pathway for UDP-N-acetylglucosamine synthesis. J. Bacteriol. 176, 5788–5795. https://doi.org/10.1128/jb.176.18.5788-5795.1994

Meyer, D., Schneider-Fresenius, C., Horlacher, R., Peist, R., Boos, W., 1997. Molecular characterization of glucokinase from Escherichia coli K-12. J. Bacteriol. 179, 1298–1306. https://doi.org/10.1128/jb.179.4.1298-1306.1997

Mirdita, M., Schütze, K., Moriwaki, Y., Heo, L., Ovchinnikov, S., Steinegger, M., 2022. ColabFold: making protein folding accessible to all. Nat. Methods 19, 679–682. https://doi.org/10.1038/s41592-022-01488-1

Miyakoshi, M., 2024. Multilayered regulation of amino acid metabolism in *Escherichia coli*. Curr. Opin. Microbiol. 77, 102406. https://doi.org/10.1016/j.mib.2023.102406

Mobley, H.L., Hausinger, R.P., 1989. Microbial ureases: significance, regulation, and molecular characterization. Microbiol. Rev. 53, 85–108. https://doi.org/10.1128/mr.53.1.85-108.1989

Morita, T., El-Kazzaz, W., Tanaka, Y., Inada, T., Aiba, H., 2003. Accumulation of Glucose 6-Phosphate or Fructose 6-Phosphate Is Responsible for Destabilization of Glucose Transporter mRNA in*Escherichia coli* *. J. Biol. Chem. 278, 15608–15614. https://doi.org/10.1074/jbc.M300177200

Niranda-Rjos, J., Saàanchez-Pescador, R., Urdea, M., Covarrubias, A.A., 1987. The complete nucleotide sequence of the ginALG operon of Escherichia coli K12. Nucleic Acids Res. 15, 2757–2770. https://doi.org/10.1093/nar/15.6.2757

Palur, D.S.K., Luu, B., Taylor, J.E., Singhal, M., Didzbalis, J., Siegel, J.B., Atsumi, S., 2025. Microbial production of D-mannose and D-sedoheptulose with tunable ratios. Trends Biotechnol. 43, 3154–3171. https://doi.org/10.1016/j.tibtech.2025.07.017

687 Pan, S., Wu, S., Kim, J., 2011. Preparation of glucosamine by hydrolysis of chitosan with
688 commercial α-amylase and glucoamylase. J. Zhejiang Univ. Sci. B 12, 931–934.
689 https://doi.org/10.1631/jzus.B1100065
690 Park, H., Bradley, P., Greisen, P.Jr., Liu, Y., Mulligan, V.K., Kim, D.E., Baker, D., DiMaio, F.,
691 2016. Simultaneous Optimization of Biomolecular Energy Functions on Features
692 from Small Molecules and Macromolecules. J. Chem. Theory Comput. 12, 6201–
693 6212. https://doi.org/10.1021/acs.jctc.6b00819
694 Passaro, S., Corso, G., Wohlwend, J., Reveiz, M., Thaler, S., Somnath, V.R., Getz, N.,
695 Portnoi, T., Roy, J., Stark, H., Kwabi-Addo, D., Beaini, D., Jaakkola, T., Barzilay, R.,
696 2025. Boltz-2: Towards Accurate and Efficient Binding Affinity Prediction.
697 https://doi.org/10.1101/2025.06.14.659707
698 Plumbridge, J., Vimr, E., 1999. Convergent Pathways for Utilization of the Amino Sugars N-
699 Acetylglucosamine, N-Acetylmannosamine, and N-Acetylneuraminic Acid by
700 Escherichia coli. J. Bacteriol. 181, 47–54. https://doi.org/10.1128/jb.181.1.47-
701 54.1999
702 Protity, A.T., Zhou, S., 2025. Recent advancement of glucosamine and N-acetyl
703 glucosamine production using microorganisms: A review. J. Ind. Microbiol.
704 Biotechnol. 52, kuaf014. https://doi.org/10.1093/jimb/kuaf014
705 Reitzer, L., 2003. Nitrogen Assimilation and Global Regulation in *Escherichia coli*. Annu.
706 Rev. Microbiol. 57, 155–176.
707 https://doi.org/10.1146/annurev.micro.57.030502.090820
708 Taylor, J.E., Palur, D.S.K., Zhang, A., Gonzales, J.N., Arredondo, A., Coulther, T.A., Lechner,
709 A.B.J., Rodriguez, E.P., Fiehn, O., Didzbalis, J., Siegel, J.B., Atsumi, S., 2023.
710 Awakening the natural capability of psicose production in Escherichia coli. Npj Sci.
711 Food 7, 54. https://doi.org/10.1038/s41538-023-00231-0
712 Teplyakov, A., Leriche, C., Obmolova, G., Badet, B., Badet-Denisot, M.-A., 2002. From Lobry
713 de Bruyn to enzyme-catalyzed ammonia channelling: molecular studies of D-
714 glucosamine-6P synthase. Nat. Prod. Rep. 19, 60–69.
715 https://doi.org/10.1039/B103713G

Teplyakov, A., Obmolova, G., Badet-Denisot, M.-A., Badet, B., Polikarpov, I., 1998. Involvement of the C terminus in intramolecular nitrogen channeling in glucosamine 6-phosphate synthase: evidence from a 1.6 å crystal structure of the isomerase domain. Structure 6, 1047–1055. https://doi.org/10.1016/S0969-2126(98)00105-1

Uehara, T., Suefuji, K., Jaeger, T., Mayer, C., Park, J.T., 2006. MurQ Etherase Is Required by Escherichia coli in Order To Metabolize Anhydro-N-Acetylmuramic Acid Obtained either from the Environment or from Its Own Cell Wall. J. Bacteriol. 188, 1660–1662. https://doi.org/10.1128/JB.188.4.1660-1662.2006

Västermark, Å., Saier, M.H., 2014. The Involvement of Transport Proteins in Transcriptional and Metabolic Regulation. Curr. Opin. Microbiol. 0, 8–15. https://doi.org/10.1016/j.mib.2014.01.002

Vo, J., Inwood, W., Hayes, J.M., Kustu, S., 2013. Mechanism for nitrogen isotope fractionation during ammonium assimilation by Escherichia coli K12. Proc. Natl. Acad. Sci. 110, 8696–8701. https://doi.org/10.1073/pnas.1216683110

White, R.J., Pasternak, C.A., 1967. The purification and properties of N-acetylglucosamine 6-phosphate deacetylase from Escherichia coli. Biochem. J. 105, 121–125. https://doi.org/10.1042/bj1050121

Woolfolk, C.A., Stadtman, E.R., 1967. Regulation of glutamine synthetase: III. Cumulative feedback inhibition of glutamine synthetase from Escherichia coli. Arch. Biochem. Biophys. 118, 736–755. https://doi.org/10.1016/0003-9861(67)90412-2

Xiong, A.-S., Yao, Q.-H., Peng, R.-H., Li, X., Fan, H.-Q., Cheng, Z.-M., Li, Y., 2004. A simple, rapid, high-fidelity and cost-effective PCR-based two-step DNA synthesis method for long gene sequences. Nucleic Acids Res. 32, e98. https://doi.org/10.1093/nar/gnh094

Yang, P., Ke, M., Feng, J., Zheng, Z., Jiang, S., 2025. Engineered Saccharomyces cerevisiae for the Enhancement of Glucosamine Accumulation by the Consumption of Glucose and Ammonium Based on Synthetic Biological Pathways. Foods 14, 2783. https://doi.org/10.3390/foods14162783

744 Yoneda, H., Tantillo, D.J., Atsumi, S., 2014. Biological Production of 2-Butanone in
745 Escherichia coli. ChemSusChem 7, 92–95. https://doi.org/10.1002/cssc.201300853
746 Yu, B., Wu, W., Wang, B., Zhang, N., Bak, K.H., Soladoye, O.P., Aluko, R.E., Zhang, Y., Fu, Y.,
747 2022. Maillard-reacted peptides from glucosamine-induced glycation exhibit a
748 pronounced salt taste-enhancing effect. Food Chem. 374, 131776.
749 https://doi.org/10.1016/j.foodchem.2021.131776
750 Zhang, J., Liu, L., Li, J., Du, G., Chen, J., 2012. Enhanced glucosamine production by
751 Aspergillus sp. BCRC 31742 based on the time-variant kinetics analysis of dissolved
752 oxygen level. Bioresour. Technol. 111, 507–511.
753 https://doi.org/10.1016/j.biortech.2012.02.063
754 Zhang, T., Yang, H., Li, G., Li, K., Liu, S., Yu, H., Xing, R., 2025. A review on the preparation
755 and synthesis strategies, mechanism and applications of different glucosamine
756 salts and derivatives. Food Biosci. 69, 106923.
757 https://doi.org/10.1016/j.fbio.2025.106923
758

Table 1 Strains used in this study.

Strain	Genotype	Source
MG1655	F- lambda- *ilvG- rfb*-50 *rph*-1	(Baba et al., 2006)
AL1050	MG1655 with attB::*lacI*^{q} *tetR* spec^{R}	(Yoneda et al., 2014)
AL4731	AL1050 with Δ*pfkA* Δ*zwf* Δ*manA* Δ*alsE* Δ*pgm* Δ*gatZ* Δ*mtlD*	(Palur et al., 2025)
AL4959	AL4731 with Δ*nagB* Δ*nagE*	This study
AL4974	AL4731 with Δ*nagB*	This study
AL4980	AL4959 with Δ*manXYZ*	This study
AL5035	AL4974 with Δ*glnE*	This study
AL5038	AL4974 with Δ*gltBD*	This study
AL5039	AL5035 with Δ*gltBD*	This study

Table 2 Plasmids used in this study

Plasmid	Description	Source
pAL2001	P_{LlacO1}:*alsE-hxpB*, amp^R, ColE1	(Taylor et al., 2023)
pAL2264	P_{LlacO1}:*galP-glk*, gent^R, p15A	(Luu et al., 2025)
pAL2333	P_{LlacO1}:*glmS-hxpB*, amp^R, ColE1	This study
pAL2344	P_{LlacO1}:*glmS*, amp^R, ColE1	This study
pAL2353	P_{LlacO1}:*glmS*(A38T), amp^R, ColE1	This study
pAL2354	P_{LlacO1}:*glmS*(A38T, R249C), amp^R, ColE1	This study
pAL2355	P_{LlacO1}:*glmS*(A38T, R249C, G471S), amp^R, ColE1	This study
pAL2434	pTargetF-*nagB*, amp^R, ColE1	This study
pAL2645	pTargetF-*manXYZ*, amp^R, ColE1	This study
pAL2816	P_{LlacO1}:*sfgfp*, kan^R, ColA	This study
pAL2937	P_{gadB}:*glmS-hxpB*, amp^R, ColE1	This study
pAL2938	P_{gadB}:*glmS-hxpA**, amp^R, ColE1	This study
pAL2939	P_{gadB}:*glmS-ybiV*, amp^R, ColE1	This study
pAL2940	P_{gadB}:*glmS-yqaB*, amp^R, ColE1	This study
pAL2941	P_{gadB}:*glmS-yidA*, amp^R, ColE1	This study
pAL2942	P_{gadB}:*glmS-yigL*, amp^R, ColE1	This study
pAL2943	P_{gadB}:*glmS-yihX*, amp^R, ColE1	This study
pAL2906	P_{gadB}:*glmS*(A38T, R249C, G471S)-*hxpB*, amp^R, ColE1	This study
pAL2907	P_{gadB}:*glmS*(A38T, R249C, G471S)-*hxpA*(1G>A)*, amp^R, ColE1	This study
pAL2908	P_{gadB}:*glmS*(A38T, R249C, G471S)-*ybiV*, amp^R, ColE1	This study
pAL2909	P_{gadB}:*glmS*(A38T, R249C, G471S)-*yqaB*, amp^R, ColE1	This study
pAL2910	P_{gadB}:*glmS*(A38T, R249C, G471S)-*yidA*, amp^R, ColE1	This study
pAL2911	P_{gadB}:*glmS*(A38T, R249C, G471S)-*yigL*, amp^R, ColE1	This study
pAL2912	P_{gadB}:*glmS*(A38T, R249C, G471S)-*yihX*, amp^R, ColE1	This study
pAL2920	P_{LlacO1}:*glnA*, kan^R, ColA	This study
pAL2998	pTargetF-*glnE*, ampR, ColE1	This study
pAL3004	P_{gadB}:*glmS*(A38T, R249C)-*ybiV*, amp^R, ColE1	This study
pAL3005	pTargetF-*gltBD*, amp^R, ColE1	This study
pAL3085	P_{gadB}:*glmS*, amp^R, ColE1	This study
pCas	P_{cas}:*cas9* P_{araB}:*red lacI*^{q} P_{trc}:sgRNA pMB1 repA101(Ts) kan^R	addgene #62225
pTargetF	PJ23119:sgRNA-pMB1, spec^R, pMB1	addgene #62226

**hxpA* carries an engineered ATG start codon (G→A substitution at the first nucleotide).

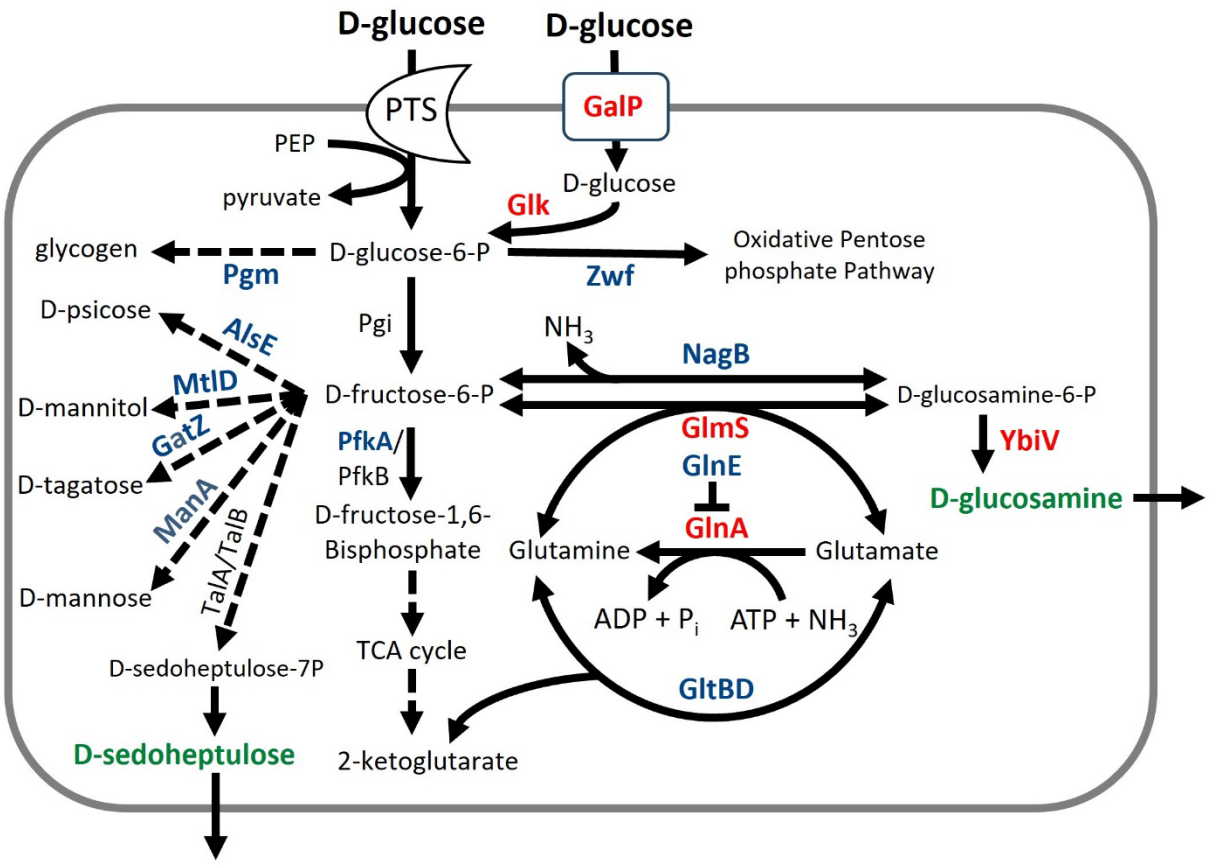

Figure 1 Phosphorylation–dephosphorylation–based biosynthesis of D-glucosamine and D-sedoheptulose.

Enzymes encoded by deleted genes are shown in blue. Enzymes encoded by additionally expressed genes are shown in red. Dotted arrowheads indicate multiple reaction steps. D-Glucosamine and D-sedoheptulose are highlighted in green.

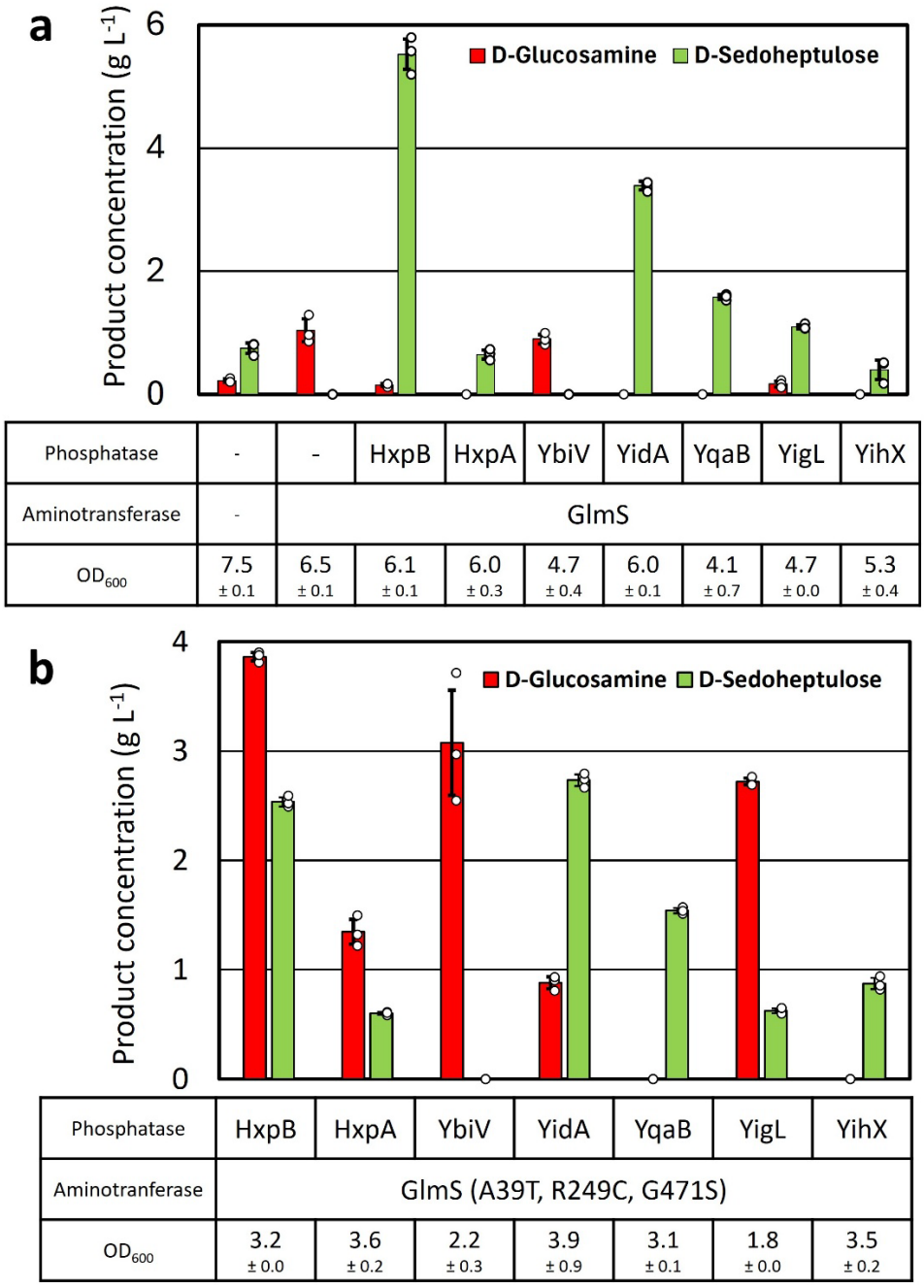

Phosphatase	-	-	HxpB	HxpA	YbiV	YidA	YqaB	YigL	YihX
Aminotransferase	-	GlmS							
OD_{600}	7.5 ± 0.1	6.5 ± 0.1	6.1 ± 0.1	6.0 ± 0.3	4.7 ± 0.4	6.0 ± 0.1	4.1 ± 0.7	4.7 ± 0.0	5.3 ± 0.4

Phosphatase	HxpB	HxpA	YbiV	YidA	YqaB	YigL	YihX
Aminotranferase	GlmS (A39T, R249C, G471S)						
OD_{600}	3.2 ± 0.0	3.6 ± 0.2	2.2 ± 0.3	3.9 ± 0.9	3.1 ± 0.1	1.8 ± 0.0	3.5 ± 0.2

Figure 2. Native D-glucosamine production in *E. coli* enabled by elimination of competing pathways and selective phosphatase activity

Cells were grown in M9P medium containing 30 g L^{-1} glucose at 37 °C to OD_{600} ≈ 1, followed by incubation at 30 °C for 24 h. D-Glucosamine and D-sedoheptulose production was evaluated in AL4731 (Δ*pfkA* Δ*zwf* Δ*alsE* Δ*manA* Δ*pgm* Δ*gatZ* Δ*mtlD*, **Table 1**) harboring plasmids encoding selected endogenous sugar phosphatases together with either (**a**) wild-type *glmS* or (**b**) *glmS* encoding feedback-insensitive GlmS54 (A38T, R249C, G471S). OD_{600} values correspond to measurements at 24 h. Error bars indicate standard deviation (n = 3 biological replicates).

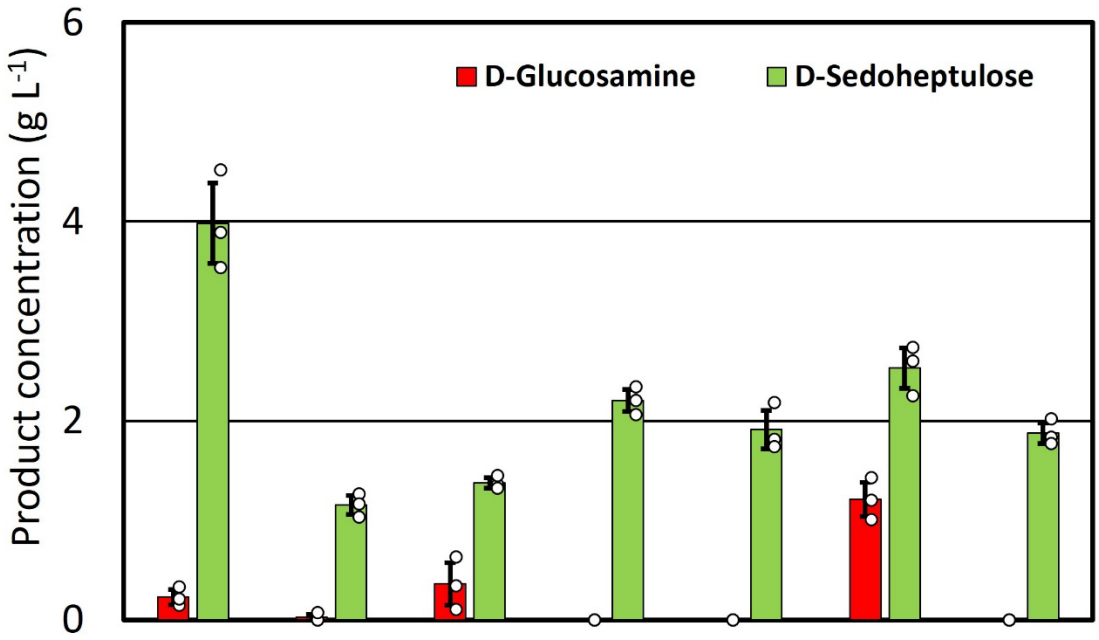

Phosphatase	HxpB	HxpA	YbiV	YidA	YqaB	YigL	YihX
Aminotranferase	GlmS (A39T, R249C, G471S)						
Glucose Importer Plasmid	GalP-Glk						
OD_{600}	1.1 ± 0.2	1.1 ± 0.0	1.7 ± 0.2	1.2 ± 0.2	4.2 ± 0.3	1.3 ± 0.2	1.1 ± 0.0

Figure 3. Effect of *galP* and *glk* additional expression on D-glucosamine Production
Cells were grown in M9P medium containing 30 g L^{-1} glucose at 37 °C to OD_{600} ≈ 1, followed by incubation at 30 °C for 24 h. At OD_{600} ≈ 1, IPTG was added to a final concentration of 1 mM when required. D-Glucosamine and D-sedoheptulose production were evaluated in AL4731 (Δ*pfkA* Δ*zwf* Δ*alsE* Δ*manA* Δ*pgm* Δ*gatZ* Δ*mtlD*, **Table 1)** harboring plasmids encoding selected sugar phosphatase genes together with *glmS* encoding GlmS54 (A38T, R249C, G471S) and the *galP-glk* expression plasmid (pAL2264, **Table 2**). OD_{600} values correspond to measurements at 24 h. Error bars indicate s.d. (n = 3 biological replicates).

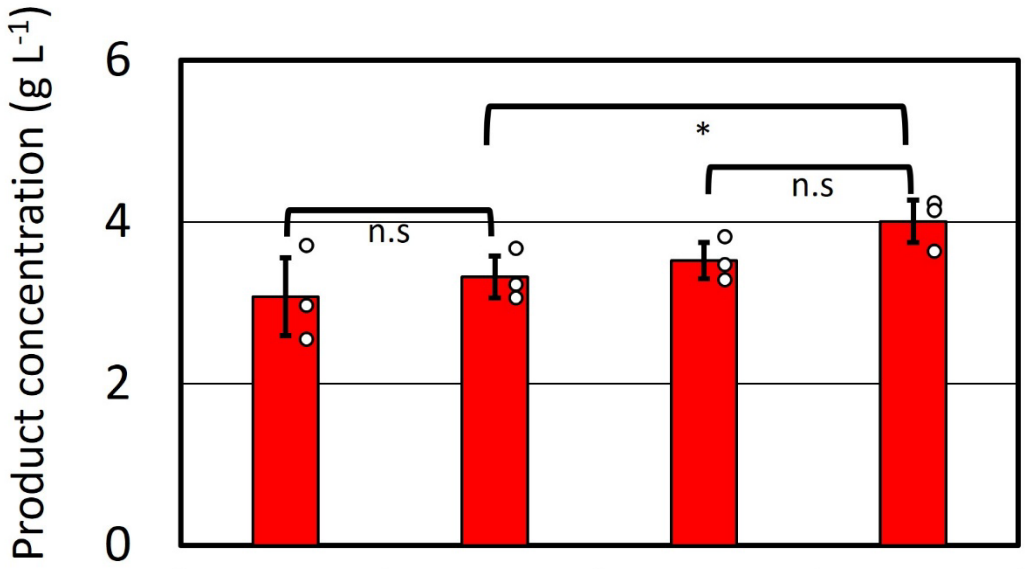

Aminotransferase	GlmS54	GlmS*	GlmS54	GlmS*
nagB	+		Δ	
OD_{600}	2.2 ± 0.3	2.4 ± 0.0	2.2 ± 0.1	2.4 ± 0.1

Figure 4. Effect of deletion of *nagB* and overexpression of *glmS on D-glucosamine production.** Cells were grown in M9P medium with 30 g L^{-1} glucose at 37 °C to OD_{600} ~1, then grown at 30 °C for 24 h. At OD_{600} ~1, 1 mM IPTG was added. D-glucosamine production was evaluated in AL4731 (Δ*pfkA* Δ*zwf* Δ*alsE* Δ*manA* Δ*pgm* Δ*gatZ* Δ*mtlD*, **Table 1)** or AL4974 (Δ*pfkA* Δ*zwf* Δ*alsE* Δ*manA* Δ*pgm* Δ*gatZ* Δ*mtlD* Δ*nagB*, **Table 1**) harboring plasmids encoding either *glmS* (GlmS54; A38T, R249C, G471S; pAL2908) or *glmS* (GlmS*; A38T, R249C; pAL3004) (**Table 2**). OD_{600} values correspond to measurements at 24 h. Error bars indicate s.d. (n = 3 biological replicates). One-way ANOVA with Dunnett's multiple comparisons test (two-sided) was used. n.s., P > 0.05; *P ≤ 0.05; **P ≤ 0.01.

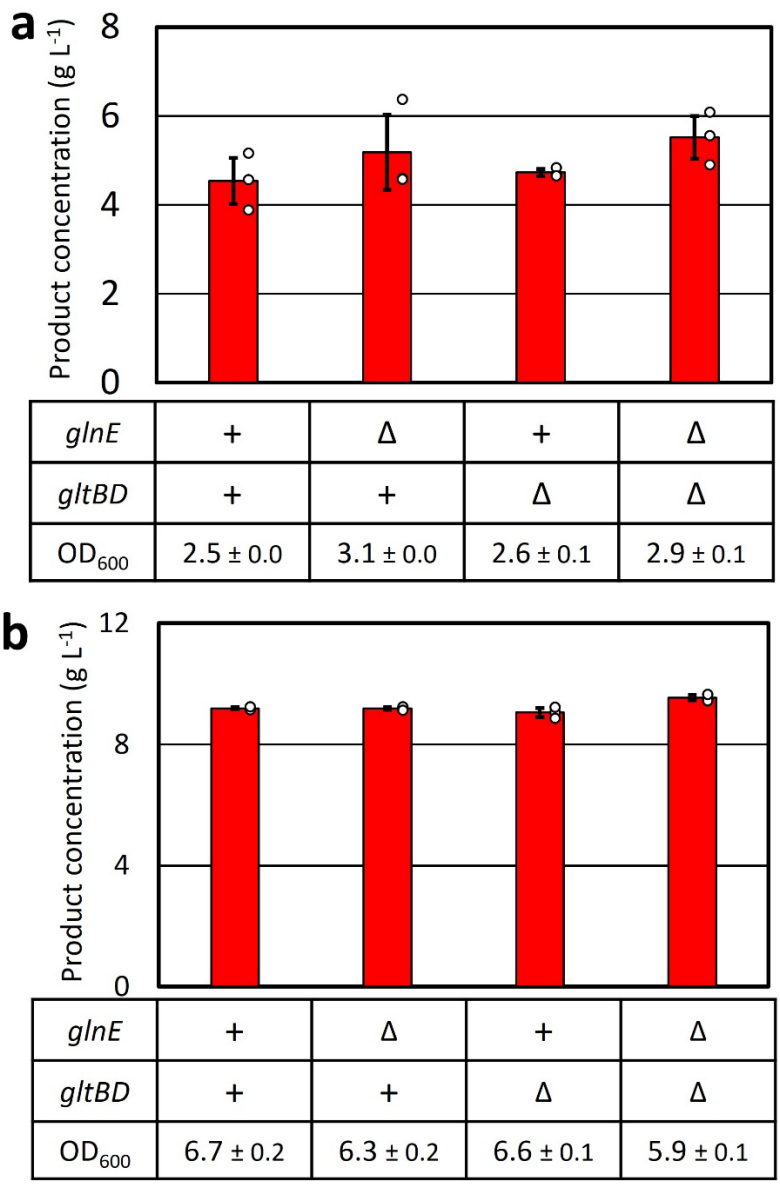

Figure 5. Modulation of the GS–GOGAT network and glutamine biosynthesis for enhanced D-glucosamine production

Cells were grown in M9YT medium containing 30 g L^{-1} glucose at 37 °C to OD_{600} ≈ 1, followed by incubation at 30 °C for 24 h. At OD_{600} ≈ 1, IPTG was added to a final concentration of 1 mM. D-Glucosamine production was evaluated in AL4974 (Δ*pfkA* Δ*zwf* Δ*alsE* Δ*manA* Δ*pgm* Δ*gatZ* Δ*mtlD* Δ*nagB*), AL5035 (AL4974 Δ*glnE*), AL5038 (AL4974 Δ*gltBD*), and AL5039 (AL4974 Δ*glnE* Δ*gltBD*) (**Table 1**). (**a**) Effect of GS–GOGAT disruption. Strains harbor pAL3004 and pAL2264 (**Table 2**). (**b**) Effect of *glnA* additional expression. Strains harbor pAL3004 and pAL2920 (**Table 2**). OD_{600} values correspond to measurements at 24 h. Error bars indicate standard deviation (n = 3 biological replicates). One-way ANOVA with Dunnett's multiple comparisons test (two-sided) was used. n.s., P > 0.05; *P ≤ 0.05; **P ≤ 0.01.

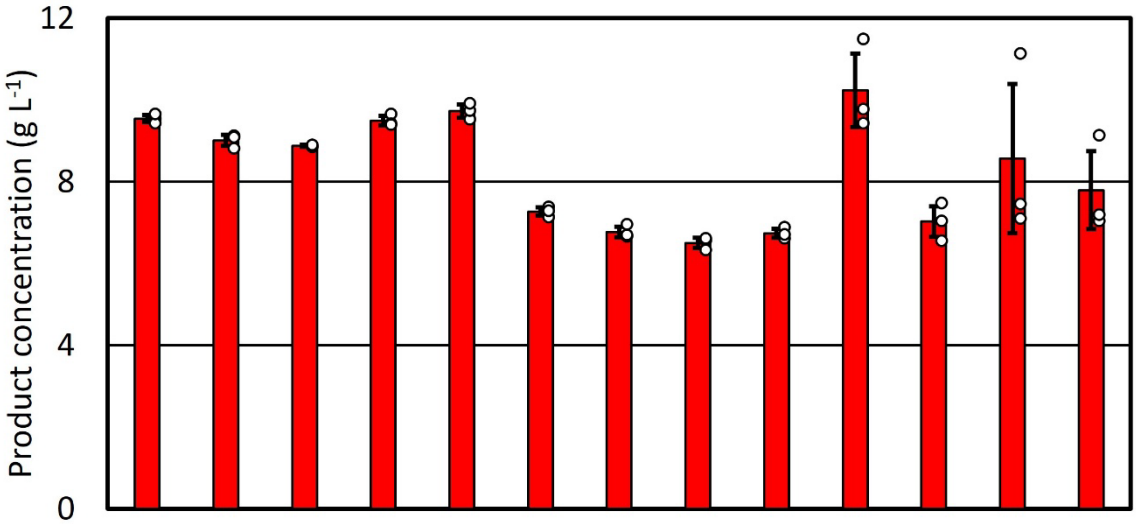

Concentration (g L^{-1})	-	1	2	5	10	1	2	5	10	1	2	5	10
Nitrogen source	-	Urea				Ammonium Chloride				L-Glutamine			
OD_{600}	5.9 ± 0.1	6.0 ± 0.4	6.1 ± 0.4	6.1 ± 0.4	6.7 ± 0.1	5.7 ± 0.2	5.2 ± 0.1	5.2 ± 0.1	5.4 ± 0.1	5.9 ± 0.3	5.9 ± 0.2	5.8 ± 0.2	5.5 ± 0.1

Figure 6. Effect of nitrogen supplementation on D-glucosamine production

Cells were grown in M9YT medium containing 30 g L^{-1} glucose supplemented with urea or ammonium chloride at the indicated concentrations. Cultures were incubated at 37 °C to $OD_{600} \approx 1$, followed by incubation at 30 °C for 24 h. At $OD_{600} \approx 1$, IPTG was added to a final concentration of 1 mM. D-Glucosamine production was evaluated in AL5039 (Δ*pfkA* Δ*zwf* Δ*alsE* Δ*manA* Δ*pgm* Δ*gatZ* Δ*mtlD* Δ*nagB* Δ*glnE* Δ*gltBD*, **Table 1**) harboring pAL3004 and pAL2920 (**Table 2**). OD_{600} values correspond to measurements at 24 h. Error bars indicate standard deviation (n = 3 biological replicates).